ARTICLES
PUBLISHED ONLINE: 5 JUNE 2011 | DOI: 10.1038/NCHEM.1067
nature chemistry

Light-induced spin-crossover magnet

Shin-ichi Ohkoshi[1,2]*, Kenta Imoto[1], Yoshihide Tsunobuchi[1], Shinjiro Takano[1] and Hiroko Tokoro[1]

The light-induced phase transition between the low-spin (LS) and high-spin (HS) states of some transition-metal ions has been extensively studied in the fields of chemistry and materials science. In a crystalline extended system, magnetically ordering the HS sites of such transition-metal ions by irradiation should lead to spontaneous magnetization. Previous examples of light-induced ordering have typically occurred by means of an intermetallic charge transfer mechanism, inducing a change of valence of the metal centres. Here, we describe the long-range magnetic ordering of the extended Fe^{II}(HS) sites in a metal–organic framework caused instead by a light-induced excited spin-state trapping effect. The Fe–Nb-based material behaves as a spin-crossover magnet, in which a strong superexchange interaction (magnetic coupling through non-magnetic elements) between photo-produced Fe^{II}(HS) and neighbouring Nb^{IV} atoms operates through CN bridges. The magnetic phase transition is observed at 20 K with a coercive field of 240 Oe.

Octahedral transition-metal complexes of d^4 to d^7 can change their spin state from high spin (HS) to low spin (LS) with a decrease in temperature; for example, $Fe^{II}_{HS}(S=2)$ is converted into $Fe^{II}_{LS}(S=0)$. Since the discovery of this phenomenon[1–13] in a Fe(III) complex, a large number of spin-crossover compounds have been reported. Their colour, and electric and magnetic properties, can be altered by external stimuli, which makes them particularly promising for applications such as memory storage.

In particular, inducing a phase transition from LS to HS by means of light irradiation (known as the light-induced excited spin-state trapping (LIESST) effect) has attracted much attention[14–23] since its discovery in a Fe(II) complex ($[Fe^{II}(1\text{-propyltetrazole})_6](BF_4)_2$) in 1984 (ref. 14). If all the HS sites of a three-dimensional extended network could be ordered in this manner, a ferromagnetic phase transition (transformation from a non-magnetically ordered phase to a magnetically ordered one) would be observed, which should lead to spontaneous magnetization. However, reported examples of photo-induced spontaneous magnetization have so far relied instead on an intermetallic charge transfer mechanism, which means that the transition-metal centres undergo a valence change in the process.

Studies to optically control ferromagnetism (the spontaneous magnetization of condensed matters) were first conducted in 1967. Light-induced changes in the initial permeability (μ, the degree of magnetization when an external magnetic field is initially applied) and coercive field (H_c, the magnetic field that reduces the magnetization of the magnet to zero) of a silicon-doped material (silicon-doped yttrium iron garnet) were triggered[24] by optical charge transfer from Fe^{II} to Fe^{III} sites[24,25].

In the past 15 years, photo-induced magnetization has been reported in several cyano-bridged metal assemblies[26–33]. In these materials, light irradiation can control the saturation magnetization (M_s, maximum magnetization), Curie temperature (T_C, long-range magnetic ordering temperature), H_c and/or the magnetic pole, which are commonly triggered by light-induced metal-to-metal charge transfer (MMCT). An optical decrease in the magnetization has also been reported in vanadium-based molecular magnets[34,35]. In systems where a photochromic molecule penetrates the ferromagnetic framework[36,37] or single-molecule magnet[38], an optical change in H_c or a.c. magnetic susceptibility has been observed through photo-isomerization. A very recent report describes a unique example of the photochromic system, with room-temperature optical switching between diamagnetic and paramagnetic nickel ions in solution[39]. Ferromagnetic ordering due to photogenerated carriers in magnetic semiconductor heterostructures layers has also been reported[40].

The LIESST effect has been reported in binuclear and tetranuclear spin-crossover complexes, and magnetic coupling between light-induced HS states has also been observed[20–23]. To extend this phenomenon to a three-dimensional magnetic network and achieve photo-induced spontaneous magnetization in a spin-crossover material, it is necessary to choose a material that features a large number of HS states with strong exchange coupling. The LIESST effect is an intra-atomic phenomenon, and a LIESST site can thus be considered a useful switching moiety for the development of advanced photomagnetism, for example for applications such as organic–inorganic hybridized photomagnetic polymers or flexible photomagnetic memory.

We have focused on the octacyanoniobate cyano-bridged metal–organic framework[41–44]. We now report the photo-induced spontaneous magnetization of an Fe–Nb-based metal–organic framework. The magnetic ordering of the Fe(II) centres, through the $-NC-Nb^{IV}(S=1/2)-CN-$ bridges, leads to pronounced magnetic ordering. We measured a magnetic phase transition temperature of 20 K and a coercive field of 240 Oe.

Results and discussion

A three-dimensional Fe–Nb bimetallic assembly, $Fe_2[Nb(CN)_8]\cdot(4\text{-pyridinealdoxime})_8\cdot 2H_2O$, was prepared by reacting a mixed aqueous solution of $FeCl_2\cdot 4H_2O$ and 4-pyridinealdoxime with an aqueous solution of $K_4[Nb(CN)_8]\cdot 2H_2O$ (see Methods).

The X-ray diffraction (XRD) powder pattern indicated that the resulting compound had a tetragonal structure ($a=20.2001(4)$ Å and $c=14.9565(5)$ Å) (Fig. 1a–c, Supplementary Figs S1–S3 and Table S1) based on Rietveld analysis using an analogous Mn–Nb compound as a reference sample (see Methods; Supplementary Figs S4, S5 and Table S2). The coordination geometries of the Fe and Nb sites were pseudo-octahedral and dodecahedral, respectively. The two axial positions of Fe were occupied by cyanide nitrogen atoms of $[Nb^{IV}(CN)_8]$, and the equatorial positions were occupied by the four nitrogen atoms of 4-pyridinealdoxime. The four CN groups of $[Nb^{IV}(CN)_8]$ were bridged to four Fe atoms,

[1]Department of Chemistry, School of Science, The University of Tokyo, 7-3-1 Hongo, Bunkyo-ku, Tokyo 113-0033, Japan, [2]CREST, JST, 5 Sanbancho, Chiyoda-ku, Tokyo 102-0075, Japan. *e-mail: ohkoshi@chem.s.u-tokyo.ac.jp

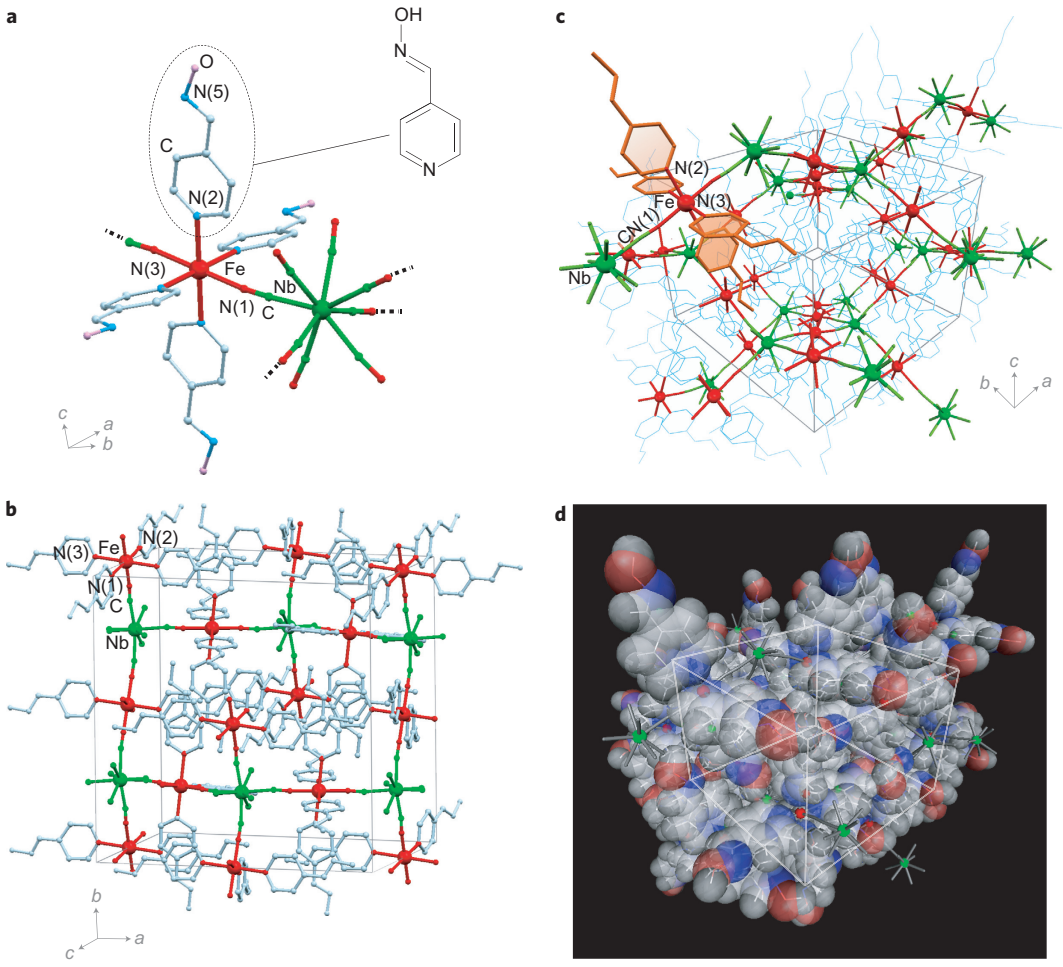

Figure 1 | Crystal structure of $Fe_2[Nb(CN)_8]\cdot(4\text{-pyridinealdoxime})_8\cdot 2H_2O$. a, Coordination environments around Fe and Nb. The Fe atom is coordinated by two cyanide nitrogen atoms of $[Nb^{IV}(CN)_8]$ and four pyridyl nitrogen atoms of 4-pyridinealdoxime. Four CN groups of $[Nb^{IV}(CN)_8]$ are bridged to four Fe centres, and the other four remain free. Red and green ball-sticks represent the $[FeN_6]$ and $[NbC_8]$ moieties, respectively. Light blue, blue and pink balls represent C, N and O atoms in 4-pyridinealdoxime. **b**, Cyano-bridged Fe–Nb three-dimensional framework viewed along the *c*-axis. **c**, View from the diagonal direction. 4-Pyridinealdoxime molecules are drawn as light blue wire frames or orange sticks with planes. Zeolitic water molecules are omitted for clarity. **d**, Organic ligand molecules of 4-pyridinealdoxime are drawn as spheres, considering their van der Waals radii. Light grey, grey, blue and red spheres denote C, H, N and O atoms, respectively. Small red and green balls and grey sticks represent Fe and Nb atoms and the cyano-bridged Fe–Nb framework, respectively.

and the other four CN groups were free. The cyano-bridged Fe–Nb formed a three-dimensional cyano-bridged bimetallic framework, which contained three types of hydrogen bonds: those between the hydroxyl group of 4-pyridinealdoxime and the non-bridged cyano nitrogens of $Nb(CN)_8$, those between the hydroxyl group of 4-pyridinealdoxime and non-coordinated water molecules, and those between the hydroxyl group of 4-pyridinealdoxime and the nitrogen atoms of other 4-pyridinealdoximes (Supplementary Fig. S3). Figure 1d depicts the crystal structure of this material, with the organic ligand molecules of 4-pyridinealdoxime drawn with their van der Waals radii.

The temperature T dependence of the molar magnetic susceptibility χ_M of the present compound displayed a thermal phase transition (Fig. 2a). The product of χ_M and T was 7.15 K cm^3 mol^{-1} at 290 K (high-T form), but decreased with decreasing temperature. The $\chi_M T$ value at 50 K was 1.72 K cm^3 mol^{-1} (low-T form). The spin transition temperature $T_{1/2}$, defined as the temperature at which the material has 50% of its population in the high-T form and 50% in the low-T form, was 130 K. The $\chi_M T$ value observed during the warming process corresponded to that obtained during the cooling process at each temperature. The electron spin resonance (ESR) spectrum showed that the gyromagnetic ratio g-value of Nb^{IV} was 1.99 (Supplementary Fig. S6). As the temperature decreased, the variable-temperature UV–vis absorption spectra exhibited optical absorptions at 480 nm (band I) and 650 nm (band II), which were assigned to the $^1A_1 \rightarrow {}^1T_2$ and $^1A_1 \rightarrow {}^1T_1$ transitions on the $Fe^{II}_{LS}(S=0)$ site, respectively (Fig. 2b, Supplementary Fig. S7). Therefore, the transition from the high-T form to the low-T form in the $\chi_M T$ versus T plots is due to the spin-crossover from Fe^{II}_{HS} to Fe^{II}_{LS}.

In the variable-temperature XRD measurements, both the lattice constants and compression of the Fe–N bond lengths, 2.03 (300 K) → 1.90 Å (20 K) on Fe–N(1), 2.26 → 2.12 Å on Fe–N(2), and 2.29 → 2.07 Å on Fe–N(3), decreased (Supplementary Figs S8, S9 and Table S3), supporting a $Fe^{II}_{HS} \rightarrow Fe^{II}_{LS}$ phase transition. Furthermore, to confirm the Fe^{II} spin-crossover, the ^{57}Fe Mössbauer spectra were measured. In the high-T form, a doublet due to Fe^{II}_{HS} (isomer shift, 1.03 mm s^{-1}; quadrupole splitting, 1.85 mm s^{-1}) was observed, whereas the low-T form was mainly composed of a doublet due to Fe^{II}_{LS} (isomer shift, 0.52 mm s^{-1}; quadrupole splitting, 0.68 mm s^{-1}) (Supplementary Fig. S10). From analysis of the $\chi_M T$ versus T plots and Mössbauer spectra, the electronic states of the high-T and low-T forms in the present spin-crossover compound were assigned to $(Fe^{II}_{HS})_2[Nb^{IV}(CN)_8]\cdot(4\text{-pyridinealdoxime})_8\cdot 2H_2O$

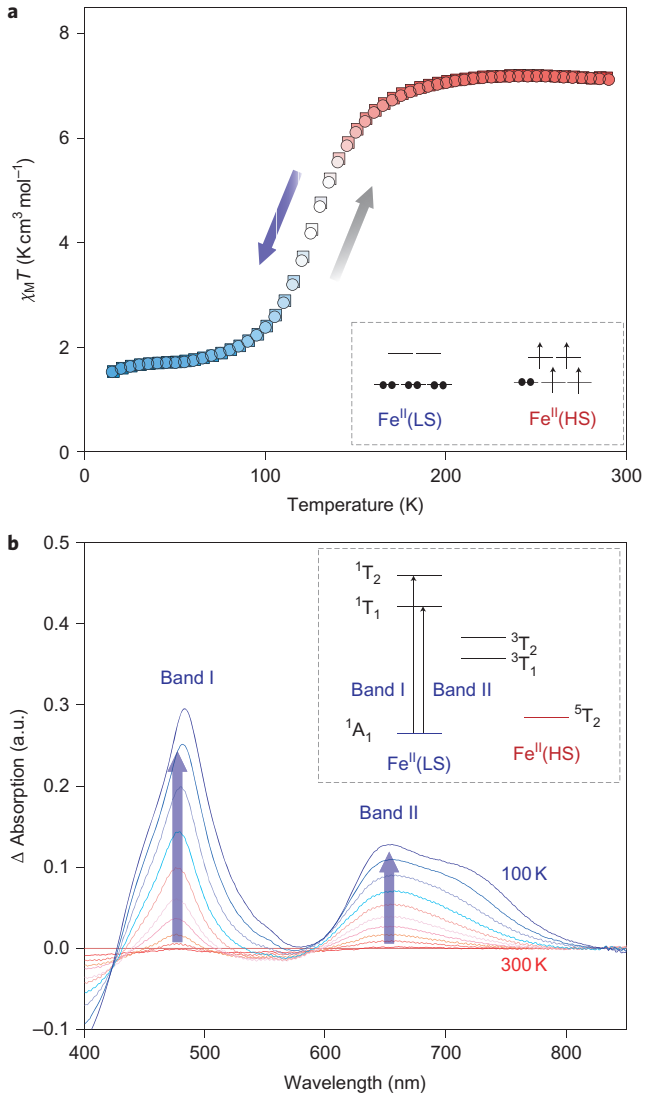

Figure 2 | Spin-crossover transition phenomenon. a, Temperature T dependence of the molar magnetic susceptibility χ_M measured in an external field of 5,000 Oe. The decrease in the $\chi_M T$ value with decreasing temperature indicates the transition from the high-T form to the low-T form, which is due to the spin-crossover from Fe^{II}(HS)($S=2$) to Fe^{II}(LS)($S=0$). Squares and circles denote $\chi_M T$ values with decreasing (blue arrow) and increasing (black arrow) temperature, respectively. Inset: schematic illustration of the electronic configuration of Fe^{II}(HS) and Fe^{II}(LS). **b**, Temperature dependencies of the differential UV–vis absorption spectra from 300 K to 100 K in 20 K intervals. As the temperature decreases, the variable-temperature UV–vis absorption spectra exhibit optical absorptions around 480 nm (band I) and 650 nm (band II). Inset: schematic illustration for the ground and excited states of Fe^{II}. Arrows indicate the d–d transitions of band I ($^1A_1 \rightarrow {}^1T_2$) and band II ($^1A_1 \rightarrow {}^1T_1$) on Fe^{II}(LS). Measurement errors are included within the marks and lines.

and $(Fe^{II}_{HS})_{0.44}(Fe^{II}_{LS})_{1.56}[Nb^{IV}(CN)_8]\cdot(4\text{-pyridinealdoxime})_8\cdot 2H_2O$, respectively (see Supplementary Information and Supplementary Fig. S11).

The photomagnetic effect of the present compound was then investigated. Because the low-T form had an absorption band due to the $^1A_1 \rightarrow {}^1T_2$ transition of Fe^{II}_{LS} at 480 nm, the low-T form was irradiated with 473 nm diode laser light (17 mW cm^{-2}, 5 min) at 2 K. Consequently, a large spontaneous magnetization was observed. The magnetization versus temperature curve produced a T_C of 20 K (Fig. 3a), while the magnetization versus external magnetic field plots exhibited a magnetic hysteresis loop with H_c of 240 Oe at 2 K (Fig. 3b). The M_s at 7 T was 7.4μ_B, which was close to the theoretical M_s value of 7.7μ_B due to ferrimagnetic coupling (long-range antiparallel ordering of the unequal magnetic centres) between Nb^{IV}($S=1/2$) and the photo-produced Fe^{II}_{HS}($S=2$) with g-values of $g_{Nb^{IV}}=1.99$ and $g_{Fe^{II}HS}=2.17$ (Supplementary Fig. S12). After termination of the irradiation, a part of the magnetization gradually relaxed but 70% of the photo-produced magnetization ultimately remained (see Methods and Supplementary Fig. S13). Upon irradiation with light, the absorption bands of the $^1A_1 \rightarrow {}^1T_2$ and $^1A_1 \rightarrow {}^1T_1$ transitions on Fe^{II}_{LS} decreased (Supplementary Fig. S14). Moreover, irradiation increased Fe^{II}_{HS}, but decreased Fe^{II}_{LS} in the Mössbauer spectra (Supplementary Fig. S15), indicating that the observed magnetization is due to a photo-induced spin-crossover from Fe^{II}_{LS} to Fe^{II}_{HS}.

The observed photomagnetism can be explained by the following scheme. Before irradiation, paramagnetic Nb^{IV} (which has unpaired electrons without long-range ordering) and diamagnetic Fe^{II}_{LS} (which does not have any unpaired electrons) of the low-T form were connected by a CN ligand in an alternating fashion, and exhibited paramagnetism. Irradiation with 473 nm light caused a LIESST effect[14–23] on the Fe^{II} site (Fig. 4a); the $^1A_1$ state on Fe^{II}_{LS} transits to

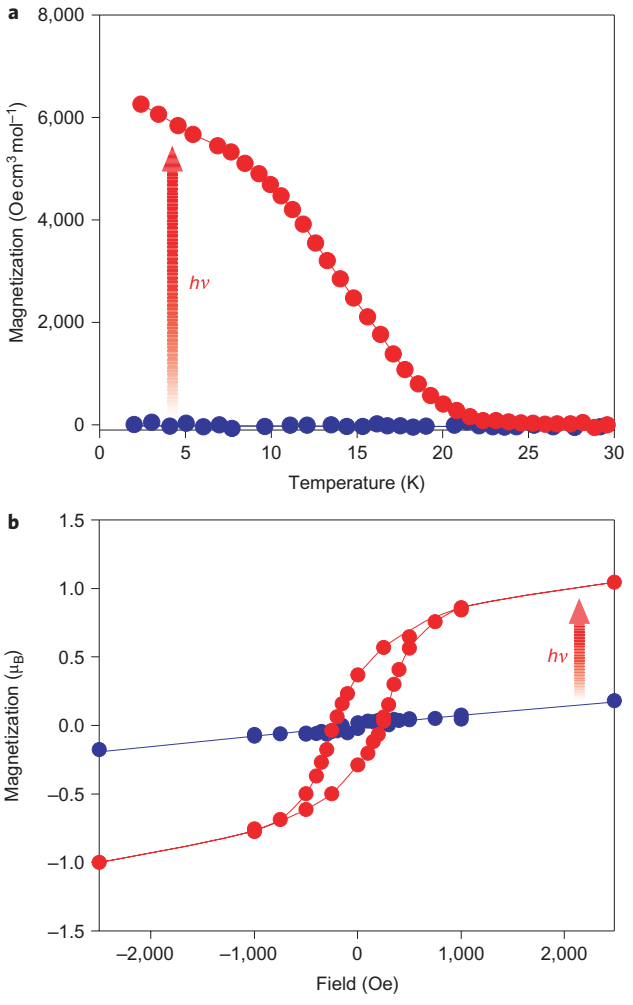

Figure 3 | Photo-induced magnetization caused by light-induced spin-crossover. a, Magnetization versus temperature curves at 100 Oe. Light irradiation induces a spontaneous magnetization with a Curie temperature of 20 K. **b**, Magnetic hysteresis curves at 2 K. After irradiation, a magnetic hysteresis loop with a coercive field of 240 Oe appeared. Blue and red circles denote measurements before and after irradiation with 473 nm light. Measurement error is included within the marks.

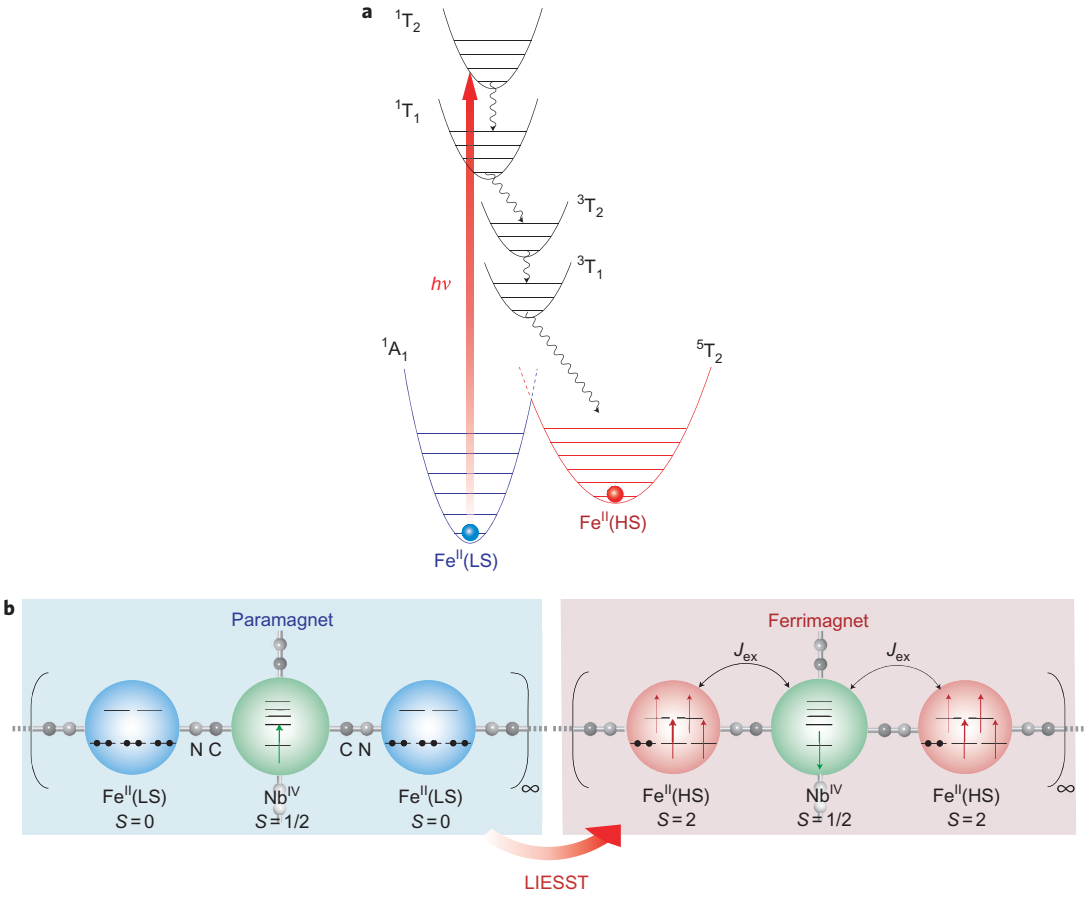

Figure 4 | Mechanism of light-induced spin-crossover ferromagnetism. a, Schematic of light-induced spin-crossover of Fe^{II}, that is, the LIESST effect. The $^1A_1$ state on Fe^{II}(LS) transits to the excited singlet state $^1T_2$ (or $^1T_1$) due to light irradiation, and then partially proceeds to the metastable quintet state $^5T_2$ through the triplet states of $^3T_2$ and $^3T_1$. **b**, Schematic of ferrimagnetic ordering between Nb^{IV}($S = 1/2$) and Fe^{II}_{HS}($S = 2$) due to light-induced spin-crossover. In the photo-induced phase, the magnetic spins on the photo-produced Fe^{II}(HS)($S = 2$) and neighbouring Nb^{IV}($S = 1/2$) interact antiferromagnetically by a strong superexchange interaction (J_{ex}) through the CN ligand, resulting in spontaneous magnetization. Black bars inside the spheres represent the levels of 4*d* orbitals on Nb^{IV} or 3*d* orbitals on Fe^{II}; red and green arrows represent spin.

the excited singlet state $^1T_2$ (or $^1T_1$) due to light irradiation, and then partially proceeds to the metastable quintet state $^5T_2$ through the triplet states of $^3T_2$ and $^3T_1$. In the photo-induced metastable high-*T* form, the magnetic spins on the photo-produced Fe^{II}_{HS}($S = 2$) and neighbouring Nb^{IV}($S = 1/2$) interacted antiferromagnetically (antiparallel coupling of the magnetic centres) by a strong superexchange interaction through the CN ligand, resulting in spontaneous magnetization (Fig. 4b). Based on molecular field theory, the superexchange interaction constant (J_{ex}) between Fe^{II}_{HS} and neighbouring Nb^{IV} was $-6.9\ cm^{-1}$ (see Methods), which is a large value for J_{ex}.

Conclusion

Herein, we report a light-induced spin-crossover magnet that consists of a three-dimensional Fe–Nb-based metal–organic framework ($Fe_2[Nb(CN)_8](4\text{-pyridinealdoxime})_8{\cdot}2H_2O$) with a tetragonal crystal structure. The magnetic properties (M_s, T_C and H_c) of the material are altered under light irradiation. This is caused by a combination of the LIESST effect (in which the Fe(II) centres of the metal–organic framework undergo a transition from LS to HS states) and strong superexchange interactions between the magnetic centres of Fe^{II}_{HS} and Nb^{IV} in the three-dimensional network.

Optical switching of the magnetic properties of M_s, T_C and H_c has also previously been observed in MMCT systems based on a cyano-bridged bimetal assembly. However, the mechanism of optical switching and the origin of bistability in MMCT systems differ from those in spin-crossover systems. In spin-crossover systems, bistability is explained by the difference between the ionic radii of the HS and LS states, and these two states are mixed by spin–orbital coupling at the atomic level. In contrast, in a MMCT system, bistability is caused by two states of a metal–metal bond, one in which the bond has mostly a covalent character and the other mostly ionic. These states are coupled by a combination of the transfer integral and vibronic coupling, and an intense absorption band due to MMCT appears in the visible and/or near-infrared region[45–49]. We have previously described two compounds of $CsFe[Cr(CN)_6]{\cdot}1.3H_2O$ (ref. 50) and $Fe_2[Nb(CN)_8]{\cdot}(3\text{-py}CH_2OH)_8{\cdot}4.6H_2O$ (ref. 13), in which spin-crossover and ferromagnetism (parallel magnetic order), or ferrimagnetism, coexist, but these compounds did not show the light-induced spin-crossover ferromagnetism that we observed with the Fe–Nb-based metal–organic framework in this study. Because the former has an intense MMCT absorption in the visible and near-infrared region, the *d*–*d* transition of Fe^{II}_{LS} cannot be excited by light irradiation. In the latter, the *d*–*d* transition can be excited, but the high symmetry of the crystal structure (Cubic, $Ia\bar{3}d$) results in a very stable alternating arrangement of ····HS–LS–···· and, consequently, the photo-induced HS domain cannot be formed.

These observations indicate that the following must be considered to realize LIESST-induced spontaneous magnetization: (i) the possibility of exciting the *d*–*d* transition of Fe^{II}_{LS}, (ii) a

three-dimensional network composed of magnetic spin sites linked by strong exchange coupling, and (iii) a somewhat low-symmetrical crystal structure to produce distortion as the photo-induced HS domain.

As an extension of this work, we are considering using the spin-crossover unit as an optical switching moiety to control magnetic properties such as M_s, T_C and H_c. If a spin-crossover site was bridged to a magnetic site on a molecule-based magnet or metal–organic framework[51–53], it may become possible to prepare spin-crossover moieties that would lead to a high-T_C molecule-based photomagnet[54–57] or a chiral molecule-based photomagnet.

Methods

Materials. The target sample of $Fe_2[Nb(CN)_8]\cdot(4\text{-pyridinealdoxime})_8\cdot 2H_2O$ was prepared by reacting a mixed aqueous solution of $FeCl_2\cdot 4H_2O$ (0.005 mol dm^{-3}) and 4-pyridinealdoxime (0.1 mol dm^{-3}) with an aqueous solution of $K_4[Nb(CN)_8]\cdot 2H_2O$ (0.05 mol dm^{-3}) under an argon atmosphere. The mixed solution was stirred for 1 h at room temperature, and the resulting precipitate was filtered to yield an air-stable powder (yield, 74%). Calc.: Fe, 7.8%; Nb, 6.5%; C, 47.2%; H, 3.7%; N, 23.6%. Found: Fe, 7.8%; Nb, 6.8%; C, 46.7%; H, 3.7%; N, 23.4%. The IR spectrum had two CN stretching peaks at 2,130 cm^{-1} (free Nb^{IV}–CN) and 2,151 cm^{-1} (Fe^{II}_{HS}–NC–Nb^{IV}) as well as peaks due to 4-pyridinealdoxime in the regions of 534–1,609 cm^{-1} and 2,650–3,500 cm^{-1}. Rietveld analysis of the XRD pattern at 300 K indicated that the sample had a tetragonal crystal structure in the $I4_1/a$ space group ($a = 20.2001(4)$ Å and $c = 14.9565(5)$ Å) with refinements of $R_{wp} = 1.98\%$ and $R_p = 1.52\%$ (Supplementary Figs. S1 and S2, Table S1). CCDC-820992 contains additional information in crystallographic information file format and can be obtained from the Cambridge Crystallographic Data Centre via www.ccdc.cam.ac.uk/data_request/cif. XRD and Rietveld analyses at other temperatures are described in the Supplementary Information (Supplementary Figs. S8 and S9 and Table S3).

A reference sample of $Mn_2[Nb(CN)_8]\cdot(4\text{-pyridinealdoxime})_8\cdot 0.2H_2O$, which is a new compound, was obtained as a single crystal by diffusing a mixed aqueous solution of $MnCl_2\cdot 4H_2O$ (0.034 mol dm^{-3}) and 4-pyridinealdoxime (0.67 mol dm^{-3}) with an aqueous solution of $K_4[Nb(CN)_8]\cdot 2H_2O$ (0.017 mol dm^{-3}). Calculated: Mn, 7.9; Nb, 6.7; C, 48.3; H, 3.5; N, 24.2%. Found: Mn, 7.8; Nb, 6.5; C, 48.2; H, 3.6; N, 24.3%. The IR spectrum displayed CN stretching peaks at 2131 and 2158 cm^{-1}, which were assigned to the CN stretching peaks of the non-bridged CN group (Nb^{IV}–CN) and the bridged CN group (Mn^{II}–NC–Nb^{IV}), respectively. X-ray single-crystal analysis confirmed that the crystal structure was tetragonal with an $I4_1/a$ space group ($a = 20.5155(15)$ Å, $c = 15.0907(13)$ Å, $Z = 4$) (CCDC-820991). The asymmetric unit consisted of a quarter of $[Nb(CN)_8]^{4-}$, a half of $[Mn(4\text{-pyridinealdoxime})_4]^{2+}$ and one-twentieth of water. The coordination geometries around the Nb and Mn sites were eight-coordinate dodecahedron and six-coordinate pseudo-octahedron, respectively. Four of the CN groups in $[Nb(CN)_8]^{4-}$ were bridged to Mn, and the other four CN groups were free. The cyano-bridged Mn–Nb formed a three-dimensional cyano-bridged bimetallic framework. Details about the crystal structure and magnetic properties are reported in the Supplementary Information (Supplementary Figs S4, S5 and Table S2).

Physical measurements. Elemental analyses of the Fe, Mn and Nb for the prepared materials were conducted by means of HP4500 inductively coupled plasma mass spectroscopy, while analyses of C, H and N were carried out using standard microanalytical methods. Infrared spectra were recorded on a JASCO IRT-3000 spectrometer in the 4,000–400 cm^{-1} region. XRD measurements were conducted on a Rigaku Ultima IV with Cu Kα radiation ($\lambda = 1.5406$ Å) within the range $10^\circ \leq 2\theta \leq 70^\circ$ using a Cu sample holder. Rietveld analyses were performed using the RIETAN-FP program. Magnetic measurements were obtained from polycrystalline samples using a Quantum Design MPMS superconducting quantum interference device (SQUID) magnetometer. The UV–vis absorption spectra were measured using a Shimadzu UV-3100 spectrometer and a JASCO MSV-370 spectrometer. The optical absorption spectra of the irradiation light sources were measured by a Hamamatsu Photonics PMA-12 photonic multichannel analyser. The temperature during the optical spectrum measurements was controlled by an Oxford Instruments Microstate-He. The ^{57}Fe Mössbauer spectra were measured using a Wissenschaftliche Elektronik Mössbauer spectrometer with a Nagase Techno-Engineering PS24SS cryostat controlling the temperature.

Photo-irradiation measurement. To investigate the magnetization changes with temperature and external magnetic fields, a diode laser with $\lambda = 473$ nm was used as the light source. The sample, which was spread on adhesive tape, was placed on the edge of an optical fibre in a SQUID. The light irradiation measurement was carried out by UV–vis absorption spectroscopy using a 473 nm diode laser light and ^{57}Fe Mössbauer spectroscopy using a xenon lamp (>420 nm).

Estimated superexchange constant based on molecular field theory. The superexchange interaction constant ($J_{ex,ij}$) on a spin Hamiltonian ($\hat{H} = -J_{ex,ij}S_i\cdot S_j$) between the i site and the nearest-neighbour j site in $(Fe^{II}_{HS})_2[Nb^{IV}(CN)_8]\cdot(4\text{-pyridinealdoxime})_8\cdot 2H_2O$ (the photo-induced phase) are related to the T_C value by the following equation:

$$T_C = \frac{|J_{ex,Fe^{II}_{HS}Nb^{IV}}|\{Z_{Nb^{IV}Fe^{II}_{HS}} Z_{Fe^{II}_{HS}Nb^{IV}} S_{Fe^{II}_{HS}}(S_{Fe^{II}_{HS}}+1) S_{Nb^{IV}}(S_{Nb^{IV}}+1)\}^{1/2}}{3k_B}$$

where S_i is the spin quantum number ($S_{Nb^{IV}} = 1/2$ and $S_{Fe^{II}_{HS}} = 2$), Z_{ij} is the number of the nearest-neighbour j sites around the i site, and k_B is the Boltzmann constant. In the case of $(Fe^{II}_{HS})_2[Nb^{IV}(CN)_8]\cdot(4\text{-pyridinealdoxime})_8\cdot 2H_2O$, $T_C = 20$ K, and Z_{ij} were $Z_{Nb^{IV}Fe^{II}_{HS}} = 4$ and $Z_{Fe^{II}_{HS}Nb^{IV}} = 2$. Consequently, $J_{ex,Fe^{II}_{HS}Nb^{IV}}$ was estimated to be -6.9 cm^{-1}.

Relaxation of the light-induced HS state. The time dependence of the light-induced HS state data at 2 K showed that the relaxation of the light-induced HS state was very slow and 70% of the initial magnetization remained. For example, after irradiation, 80% of the light-induced HS state remained after 10 h, 76% after 20 h, 74% after 30 h and ultimately 70% of the initial magnetization remained with no further decay (from fitting of the decay curve, double exponential fitting) (Supplementary Fig. S13). Although relaxation was observed after irradiation, according to the results of the magnetization versus temperature curves, on increasing the temperature above T_C and subsequently cooling to a lower temperature, the T_C value of 20 K was not influenced by this relaxation (Supplementary Fig. S16). Supplementary Fig. S17 plots the temperature dependence of the light-induced HS state. The relaxation temperature of the LIESST effect (T_{LIESST}) is difficult to determine in the present system due to the contribution of superparamagnetism above T_C (= 20 K). Thus, we defined the temperature where the photo-induced phase disappears with increasing temperature ($T_{p\downarrow}$), giving a value of $T_{p\downarrow}$ of 58 K.

Received 24 November 2010; accepted 3 May 2011; published online 5 June 2011

References

1. Gütlich, P. & Goodwin, H. A. (eds.) Spin crossover in transition metal compounds I, II, III. *Top. Curr. Chem.* **233–235** (2004).
2. König, E. Structural changes accompanying continuous and discontinuous spin-state transitions. *Prog. Inorg. Chem.* **35,** 527–622 (1987).
3. Cambi, L. & Szego, L. Über die magnetische Susceptibilität der komplexen Verbindungen. *Ber. Dtsch Ges.* **64,** 2591–2598 (1931).
4. Baker, W. A. & Bobonich, H. M. Magnetic properties of some high-spin complex of iron(II). *Inorg. Chem.* **3,** 1184–1188 (1964).
5. Kahn, O. & Martinez, C. J. Spin-transition polymers: from molecular materials toward memory devices. *Science* **279,** 44–48 (1998).
6. Real, J. A. *et al.* Spin crossover in a catenane supramolecular system. *Science* **268,** 265–267 (1995).
7. Létard, J. F. *et al.* Wide thermal hysteresis for the mononuclear spin-crossover compound *cis*-bis(thiocyanato)bis[*N*-(2′-pyridylmethylene)-4-(phenylethynyl)anilino]iron(II). *J. Am. Chem. Soc.* **119,** 10861–10862 (1997).
8. Boukheddaden, K., Shteto, I., Hoo, B. & Varret, F. Dynamical model for spin-crossover solids. I. Relaxation effects in the mean-field approach. *Phys. Rev. B* **62,** 14796–14805 (2000).
9. Bousseksou, A., Molnár, G., Demont, P. & Menegotto, J. Observation of a thermal hysteresis loop in the dielectric constant of spin crossover complexes: towards molecular memory devices. *J. Mater. Chem.* **13,** 2069–2071 (2003).
10. Niel, V. *et al.* Crystalline-state reaction with allosteric effect in spin-crossover, interpenetrated networks with magnetic and optical bistability. *Angew. Chem. Int. Ed.* **42,** 3760–3763 (2003).
11. Halder, G. J., Kepert, C. J., Moubaraki, B., Murray, K. S. & Cashion, J. D. Guest-dependent spin crossover in a nanoporous molecular framework material. *Science* **298,** 1762–1765 (2002).
12. Gaspar, A. B., Seredyuk, M. & Gütlich, P. Spin crossover in metallomesogens. *Coord. Chem. Rev.* **253,** 2399–2413 (2009).
13. Arai, M., Kosaka, W., Matsuda, T. & Ohkoshi, S. Observation of an Fe(II) spin-crossover in an iron octacyanoniobate-based magnet. *Angew. Chem. Int. Ed.* **47,** 6885–6887 (2008).
14. Decurtins, S., Gütlich, P., Köhler, C. P., Spiering, H. & Hauser, A. Light-induced excited spin state trapping in a transition-metal complex: the hexa-1-propyltetrazole–iron(II) tetrafluoroborate spin-crossover system. *Chem. Phys. Lett.* **105,** 1–4 (1984).
15. Gütlich, P., Hauser, A. & Spiering, H. Thermal and optical switching of iron(II) complexes. *Angew. Chem. Int. Ed. Engl.* **33,** 2024–2054 (1994).
16. Nasu, K. *Relaxations of Excited States and Photo-Induced Structural Phase Transitions* (Springer, 1997).
17. Létard J. F. *et al.* Structural, magnetic, and photomagnetic studies of a mononuclear iron(II) derivative exhibiting an exceptionally abrupt spin transition. Light-induced thermal hysteresis phenomenon. *Inorg. Chem.* **37,** 4432–4441 (1998).

18. Ogawa, Y. *et al.* Dynamical aspects of the photoinduced phase transition in spin-crossover complexes. *Phys. Rev. Lett.* **84,** 3181–3184 (2000).
19. Renz, F. *et al.* Strong field iron (II) complex converted by light into a long-lived high-spin state. *Angew. Chem. Int. Ed.* **39,** 3699–3700 (2000).
20. Ould-Moussa, N. *et al.* Wavelength selective light-induced magnetic effects in the binuclear spin crossover compound $\{[Fe(bt)(NCS)_2]_2(bpym)\}$. *Phys. Rev. B* **75,** 054101 (2007).
21. Ould-Moussa, N. *et al.* Selective photoswitching of the binuclear spin crossover compound $\{[Fe(bt)(NCS)_2]_2(bpm)\}$ into two distinct macroscopic phases. *Phys. Rev. Lett.* **94,** 107205 (2005).
22. Breuning, E. *et al.* Spin crossover in a supramolecular Fe_4^{II} [2×2] grid triggered by temperature, pressure, and light. *Angew. Chem. Int. Ed.* **39,** 2504–2507 (2000).
23. Nishihara, T., Nihei, M., Oshio, H. & Tanaka, K. The light-induced spin transition of tetranuclear spin crossover complex $[Fe_4(CN)_4(bpy)_4(tpa)_2](PF_6)_4$. *J. Phys.: Confer. Ser.* **148,** 012033 (2009).
24. Teale, R. W. & Temple, D. W. Photomagnetic anneal, a new magneto-optic effect, in Si-doped yittrium iron garnet. *Phys. Rev. Lett.* **19,** 904–905 (1967).
25. Enz, U. & Van der Heide, H. Two new manifestations of the photomagnetic effect. *Solid State Commun.* **6,** 347–349 (1968).
26. Sato, O., Iyoda, T., Fujishima, A. & Hashimoto, K. Photoinduced magnetization of a cobalt-iron cyanide. *Science* **272,** 704–705 (1996).
27. Shimamoto, N., Ohkoshi, S., Sato, O. & Hashimoto, K. Control of charge-transfer-induced spin transition temperature on cobalt–iron prussian blue analogues. *Inorg. Chem.* **41,** 678–684 (2002).
28. Ohkoshi, S. *et al.* Photoinduced magnetization in copper octacyanomolybdate. *J. Am. Chem. Soc.* **128,** 270–277 (2006).
29. Tokoro, H. *et al.* Visible-light-induced reversible photomagnetism in rubidium manganese hexacyanoferrate. *Chem. Mater.* **20,** 423–428 (2008).
30. Ohkoshi, S., Einaga, Y., Fujishima, A. & Hashimoto, K. Magnetic properties and optical control of electrochemically prepared iron–chromium polycyanides. *J. Electroanal. Chem.* **473,** 245–249 (1999).
31. Arimoto, Y., Ohkoshi, S., Zhong, Z. J., Seino, H., Mizobe, Y. & Hashimoto K. Photoinduced magnetization in a two-dimensional cobalt octacyanotungstate. *J. Am. Chem. Soc.* **125,** 9240–9241 (2003).
32. Ohkoshi, S., Ikeda, S., Hozumi, T., Kashiwagi, T. & Hashimoto, K. Photoinduced magnetization with a high Curie temperature and a large coercive field in a cyano-bridged cobalt–tungstate bimetallic assembly. *J. Am. Chem. Soc.* **128,** 5320–5321 (2006).
33. Ohkoshi, S. & Hashimoto, K. Design of a novel magnet exhibiting photoinduced magnetic pole inversion based on molecular field theory. *J. Am. Chem. Soc.* **121,** 10591–10597 (1999).
34. Bozdag, K. D. *et al.* Optical control of magnetization in a room-temperature magnet: V–Cr Prussian blue analog. *Phys. Rev. B* **82,** 094449 (2010).
35. Yoo, J.-W., Edelstein, R. S., Lincoln, D. M., Raju, N. P. & Epstein, A. J. Photoinduced magnetism and random magnetic anisotropy in organic-based magnetic semiconductor $V(TCNE)_x$ films, for $x\sim2$. *Phys. Rev. Lett.* **99,** 157205 (2007).
36. Bénard, S., Rivière, E., Yu, P., Nakatani, K. & Delouis, J. F. A photochromic molecule-based magnet. *Chem. Mater.* **13,** 159–162 (2001).
37. Kida, N. *et al.* Control of charge transfer phase transition and ferromagnetism by photoisomerization of spiropyran for an organic–inorganic hybrid system, $(SP)[Fe^{II}Fe^{III}(dto)_3]$ (SP = spiropyran, dto = $C_2O_2S_2$). *J. Am. Chem. Soc.* **131,** 212–220 (2009).
38. Morimoto, M., Miyasaka, H., Yamashita, M. & Irie, M. Coordination assemblies of $[Mn_4]$ single-molecule magnets linked by photochromic ligands: photochemical control of the magnetic properties. *J. Am. Chem. Soc.* **131,** 9823–9835 (2009).
39. Venkataramani, S., Jana, U., Dommaschk, M., Sönnichsen, F. D., Tuczek, F. & Herges, R. Magnetic bistability of molecules in homogeneous solution at room temperature. *Science* **331,** 445–448 (2010).
40. Koshihara, S. *et al.* Ferromagnetic order induced by photogenerated carriers in magnetic III–V semiconductor heterostructures of (In,Mn)As/GaSb. *Phys. Rev. Lett.* **78,** 4617–4620 (1997).
41. Sieklucka, B. *et al.* Towards high T_c octacyanometalate-based networks. *CrystEngComm.* **11,** 2032–2039 (2009).
42. Pinkowicz, D. *et al.* Magnetic spongelike behavior of 3D ferromagnetic $\{[Mn^{II}(imH)]_2[Nb^{IV}(CN)_8]\}_n$ with T_c=62 K. *Inorg. Chem.* **47,** 9745–9747 (2008).
43. Kosaka, W., Imoto, K., Tsunobuchi, Y. & Ohkoshi S. Vanadium octacyanoniobate-based magnet with a Curie temperature of 138 K. *Inorg. Chem.* **48,** 4604–4606 (2009).
44. Herrera, J. M. *et al.* Three-dimensional bimetallic octacyanidometalates $[M^{IV}\{(\mu\text{-}CN)_4Mn^{II}(H_2O)_2\}_2\cdot4H_2O]_n$ (M = Nb, Mo, W): synthesis, single-crystal X-ray diffraction and magnetism. *C. R. Chimie* **11,** 1192–1199 (2008).
45. Kahn, O. *Molecular Magnetism* (VCH, 1993).
46. Brown, D. B. *Mixed Valence Compounds* (NATO ASI, 1980).
47. Prassides, K. *Mixed Valency Systems: Applications in Chemistry, Physics and Biology* (NATO ASI, 1991).
48. Robin M. B. & Day P. Mixed valence chemistry—a survey and classification. *Adv. Inorg. Chem. Radiochem.* **10,** 247–422 (1967).
49. Hennig, H., Rehorek, A., Rehorek, D. & Thomas, Ph. Photocatalytic systems. LVIII. Electron transfer in copper(I)/octacyauomolybdate(V) ion pairs generated by IT excitation. *Inorg. Chim. Acta* **77,** L11–L12 (1983).
50. Kosaka, W., Nomura, K., Hashimoto, K. & Ohkoshi, S. Observation of an Fe(II) spin-crossover in a cesium iron hexacyanochromate. *J. Am. Chem. Soc.* **127,** 8590–8591 (2005).
51. Cheetham, A. K., Férey, G. & Loiseau, T. Open-framework inorganic materials. *Angew. Chem. Int. Ed.* **38,** 3269–3292 (1999).
52. Eddaoudi, M. *et al.* Modular chemistry: secondary building units as a basis for the design of highly porous and robust metal–organic carboxylate frameworks. *Acc. Chem. Res.* **34,** 319–330 (2001).
53. Kitagawa, S., Kitaura, R. & Noro, S. Functional porous coordination polymers. *Angew. Chem. Int. Ed.* **43,** 2334–2375 (2004).
54. Ferlay, S., Mallah, T., Ouahès, R., Veillet, P. & Verdaguer, M. A room-temperature organometallic magnet based on Prussian blue. *Nature* **378,** 701–703 (1995).
55. Verdaguer, M. *et al.* Room-temperature molecule-based magnets. *Phil. Trans. R. Soc. Lond. A* **357,** 2959–2976 (1999).
56. Holmes, S. M. & Girolami, G. S. Sol–gel synthesis of $KV^{II}[Cr^{III}(CN)_6]\cdot2H_2O$: a crystalline molecule-based magnet with a magnetic ordering temperature above 100 °C. *J. Am. Chem. Soc.* **121,** 5593–5594 (1999).
57. Hatlevik, Ø., Buschmann, W. E., Zhang, J., Manson, J. L. & Miller, J. S. Enhancement of the magnetic ordering temperature and air stability of a mixed valent vanadium hexacyanochromate(III) magnet to 99 °C (372 K). *Adv. Mater.* **11,** 914–918 (1999).

Acknowledgements

The authors acknowledge support from the Core Research for Evolutional Science and Technology (CREST) project of JST, a Grant-in-Aid for Young Scientists (S) from JSPS, the Global COE Program, 'Chemistry Innovation through Cooperation of Science and Engineering' from MEXT Japan, the Photon Frontier Network Program from MEXT, the Izumi Science and Technology Foundation and the Asahi Glass Foundation. The authors are grateful to Kosuke Nakagawa, Koji Nakabayashi and Tomohiro Nuida for their assistance with measurements, and to Wataru Kosaka for help with the synthesis. Acknowledgements are also given to the Cryogenic Research Center, The University of Tokyo and the Center for Nano Lithography & Analysis, The University of Tokyo, supported by MEXT Japan.

Author contributions

S.O. designed and coordinated this study, contributed to all measurements and calculations, and wrote the paper. K.I. carried out the synthesis, photo-irradiation measurements and Mössbauer spectroscopy. Y.T. conducted Rietveld analysis. S.T. performed the synthesis and elemental analysis. H.T. carried out photo-irradiation measurements and molecular-field calculations. All authors commented on the manuscript.

Additional information

The authors declare no competing financial interests. Supplementary information accompanies this paper at www.nature.com/naturechemistry. Reprints and permission information is available online at http://www.nature.com/reprints/. Correspondence and requests for materials should be addressed to S.O.